Microstructures and Failure Mechanisms of Friction Stir Spot Welds of Aluminum 6061-T6 Sheets

D.-A. Wang[a*] and S.-C. Lee[b]

[a]*Institute of Precision Engineering, National Chung Hsing University, 250 Kuo Kuang Rd, Taichung 402, Taiwan, ROC*
[b]*Mechanical & Automation Engineering, Da Yeh University, 112 Shan Jiau Rd, Da Tsuen, Chang Hua 515, Taiwan, ROC*

August 1, 2006

Abstract

Microstructures and failure mechanisms of friction stir spot welds in aluminum 6061-T6 lap-shear specimens are investigated based on experimental observations. Optical micrographs of the cross sections of friction stir spot welds in lap-shear specimens before and after failure are examined. These friction stir spot welds show the failure mode of nugget pullout under lap-shear loading conditions. The experimental observations suggest that under lap-shear loading conditions, the failure is initiated near the possible original notch tip in the stir zone (SZ) and the failure propagates along the circumference of the nugget to final fracture. Microindentation hardness data of base metal (BM), heat affected zone (HAZ), thermal-mechanical affected zone (TMAZ) and SZ are obtained. The interface between the HAZ and the TMAZ is the softest region, where the cracks of friction stir spot welds in the lap-shear specimens under the loadings initiate and lead to fracture of the specimens.

Keywords: Friction stir spot weld; Lap-shear specimen; Fracture; Microstructure

* Corresponding author: Tel.:+886-4-22857207; fax:+886-4-22858362

E-mail address: daw@nchu.edu.tw (D.-A. Wang).

1. Introduction

A rapid development of applications of lightweight materials in the automotive industry is reflected in the increasing use of aluminum and magnesium alloys. Many components produced from these alloys, by stamping, casting, extrusion and forging, have to be joined as a part of manufacturing processes. Resistance spot welding (RSW) is the most commonly used joining technique for parts made of steel sheets. The main advantages of the resistance spot welding process are its relatively low capital cost, ease of maintenance, and high tolerance to poor part fit up compared with other fusion welding technologies [1]. However, resistance spot welding of aluminum sheets by contrast has several technological challenges. First, the electrode tip life is shorter than that for welding steel sheets. Resistance spot welding of aluminum sheets is also likely to produce such defects as porosity, as reported in Thornton et al. [2] and Gean et al. [3]. Recently, a new friction stir spot welding technology has been developed by Mazda Motor Corporation and Kawasaki Heavy Industry [4,5] with much lower operating and investment cost.

A schematic illustration of the friction stir spot welding process is shown in Fig. 1 [4]. The process is applied to join two metal sheets. A rotating tool with a probe pin plunges into the upper sheet and a backing tool beneath the lower sheet supports the downward force. The downward force and the rotational speed are maintained for an appropriate time to generate frictional heat. Then, heated and softened material adjacent to

the tool deforms plastically, and a solid state bond is made between the surfaces of the upper and lower sheets.

One benefit of friction stir spot welding compared to the conventional fusion welding processes is that for aluminum-based alloys, it is possible to make joints where the strength of the weld is comparable to that of the base metal alloy. Aluminum alloys are difficult to be fusion-welded due to the requirements of (i) gas shielding of weld pool, and (ii) removal of oxide layers prior to or during the welding process [6,7]. In addition, aluminum alloys are subject to voids and solidification cracking defects when they cool from a liquid [8,9]. Therefore, friction stir spot welding offers significant performance advantages. Because melting is avoided, the energy input used for friction stir spot welding is considerably low. Consequently, the HAZs and residual stresses associated with the welds can be relatively small [1].

In this paper, microstructures and failure mechanisms of friction stir spot welds in aluminum 6061-T6 lap-shear specimens are investigated based on experimental observations. A tool with a flat tool shoulder and a cone-shaped probe pin was used. Micrographs of friction stir spot welds in lap-shear specimens before and after failure are obtained. Microstructures for friction stir spot welds are then presented. Finally, the failure mode and failure mechanism for these friction stir spot welds are discussed.

2. Experimental procedures

In this investigation, aluminum 6061-T6 sheets with a thickness of 1 mm were used. Table 1 lists the chemical compositions (wt.%) of the 6061-T6 aluminum sheets. Fig. 2 schematically shows a lap-shear specimen used to investigate the strength of friction stir spot welds under shear loading conditions. The weld nugget is idealized as a cone. The lap-shear specimen has a thickness of 1 mm, a width of 25 mm, an indentation diameter of

approximately 12 mm, an overlap length of the upper and lower sheets being 50 mm, and a length of 100 mm. As also shown in Fig. 2, two spacers with a length of 30 mm are attached to the both ends of the lap-shear specimen to induce a pure shear to the interfacial plane of the nugget for the two sheets and to avoid the initial realignment during testing. The indentation on the surface of the upper sheet of the specimen is caused by the tool plunging into the upper sheet of the specimen.

The welds were made by using a hydraulic riveting machine (LF-168, Chang Lian Fa Machinery Co., Ltd.) as shown in Fig. 3(a). A fixture was designed for friction stir spot welding of specimens. The fixture with a specimen is shown in Fig. 3(b). The specimen is mounted on a backing tool by four bolts. Granite was selected as the material for the backing tool to achieve low heat conductance through the backing tool. A load cell (CLP-5B, Tokyo Sokki Kenkyujo Co., Ltd.) was placed under the backing tool to measure the downward force during friction stir spot welding. We used a NI SCXI-1121 isolated input module with a sampling rate up to 3.33×10^5 samples/sec to acquire signals from the load cell and a NI SCXI-1600 module with a sampling rate of 200,000 samples/second and 16-bit resolution to provide data acquisition and control capabilities.

For the conventional friction stir spot welding process, the important processing parameters are the tool geometry, the rotational speed, the holding time and the downward force. As schematically shown in Fig. 4, during the friction stir spot welding process in this investigation, the rotational speed is kept constant and the downward force is controlled by the riveting machine control unit. Initially, the downward force increases almost linearly for a period of time. Then the downward force is kept nearly constant for a period of time and finally decreases almost linearly to zero. As shown in the figure, t_i represents the time that the tool contacts to the top surface of the upper sheet and t_f represents the time that tool extracts from the top surface of the upper sheet. The time between t_i and t_f

represents the total holding time. The rotational speed, constant downward force, holding time $t_f - t_i$, and force holding time for the friction stir spot welding of the specimens are 3445 rpm, 1740 N, 41 sec, and 38 sec, respectively.

Fig. 5(a) is a photo of a tool used in this investigation. The tool has a cylindrical shoulder and a cone-shaped probe. Fig. 5(b) shows a schematic plot of an extracted tool and two welded sheets after welding. The diameters of the tool shoulder and the probe pin used in this investigation are 12 mm and 5 mm, respectively. The depth of the probe pin is 1.5 mm. The angle of the chamber with the probe end surface is 10°. H is the plunge depth of the tool. The actual bonding diameter for the weld is denoted as D_c. The plunge depth, H, and the diameter of the weld, D_c, will depend upon the processing parameters.

The lap-shear specimens were then tested by using a tensile testing machine (Wain-Tsiang Ltd., Taiwan) at a monotonic displacement rate of 5.0 mm per minute. The load and displacement were simultaneously recorded during the test. Tests were terminated when the two sheets of the specimen were separated. In order to understand the relationship between failure locations and microindentation hardness variations of the friction stir spot welds, microindentation hardness data across the cross-sections of the specimens were obtained using a diamond indenter with a 1-kgf load and a 10 sec dwell time.

3. Results and discussions

Fig. 6(a) shows a lap-shear friction stir spot weld specimen. Fig. 6(b) shows a close-up top view of the friction stir spot weld on the upper sheet. As shown in the top view, the top surface of the weld looks like a button with a central hole. The squeezed-out material is accumulated along the outer circumference of the shoulder indentation. Fig. 6(c)

shows a close-up bottom view of the friction stir spot weld on the lower sheet. In the bottom view, the contact mark due to the backing tool can be seen.

In order to understand the failure mechanisms of friction stir spot welds under lap-shear loading conditions, optical micrographs of the cross sections of friction stir spot welds before and after failure were obtained. A systematic investigation of the processing parameters of holding time and constant downward force was carried out in order to obtain the friction stir spot welds of the lap-shear specimens failed in the circumferential failure mode under tensile tests. Note that the circumferential failure mode may be preferred over the interfacial failure mode. It can be explained by the higher failure loads of the friction stir spot welds in aluminum 6061-T6 lap-shear specimens failed in the circumferential mode than those failed in the interfacial mode [10]. Sawhill and Furr [11] reported similar results for the resistance spot welds of some carbon steels.

Fig. 7(a) shows a micrograph of the cross section of a friction stir spot weld before testing. Fig. 7(b) shows close-up views of regions I, II, III and IV as marked in Fig. 7(a) where the BM is not shown. In Fig. 7(a), there is an indentation with a profile that reflects the shape of the probe pin and the flat shoulder of the tool. The bottom surface is kept almost flat except near the central hole. Near the outer area of the central hole, there is a gray area which represents the SZ where the upper and lower sheets are bonded. The diameter of the nugget is nearly 6.5 mm, which is the diameter of the nearly circular gray area of the micrograph shown in Fig. 7(a). Note that for common low carbon steel, the standard nugget diameter for resistance spot welds is 5.5 mm with a 5.5 mm sheet thickness [12]. Two notch tips can be seen near points A and B. The notch tips extended into the weld appear to be formed from the unwelded interfaces between the two sheets. Note that in the SZ no defects were observed compared with the aluminum resistance spot welds where porosity was encountered.

For the friction stir spot weld made by the tool, as the tool continues to rotate and plunge into the upper and lower sheets, the material under the tool shoulder near the probe pin is stirred. Outside the SZ, the interfacial surface of the upper and lower sheets is distorted into a macroscopic curved interface as shown in region IV in Fig. 7(a). The shoulder indentation squeezes out a portion of the upper sheet material and, consequently, the thickness of the upper sheet material under the shoulder indentation decreases, resulting in a radial expansion of the upper sheet along the outer circumference of the shoulder indentation. However, due to the constraint of the neighboring material, the sheet is therefore bent along the outer circumference of the shoulder indentation. The bending of the sheet creates a gap between the upper and lower sheets. The squeezed out material from the shoulder indentation forms a ring along the outer circumference of the shoulder indentation on the top surface of the upper sheet. The squeezed out material can be seen in Fig. 7(a). In Fig. 7(b), a micrograph of the BM shows relatively coarse grains. A close-up view of region I shows less coarse grains in the HAZ than in the BM. A close-up view of regions II shows finer and distorted grains in the TMAZ. Close-up views of regions III and IV show very fine equiaxed grains in the SZ. The equiaxed grains in the SZ are probably formed due to stir and recrystallization. These equiaxed grains appeared in the SZ of friction stir welding are also reported by Liu et al. [13]. In Fig. 7(b), a close-up view of region IV shows that the curved interface becomes vague and disappears close to the SZ.

Fig. 8 shows a failed lap-shear friction stir spot weld specimen and close-up views of the friction stir spot weld in the failed lap-shear specimen. The circumferential failure mode or the nugget pullout failure mode can be seen on the lower sheet of the failed specimen in Fig. 8(a). Fig. 8(b) shows a top view of the failed friction stir spot weld. The hole diameter is almost the same as the indentation diameter D_i or the tool shoulder diameter D_t. Fig. 8(c) shows a top view of a friction stir spot weld on the lower sheet of

the failed specimen. As shown in Figs. 8(a) and 8(c), a small portion near the left hand side of the remaining weld nugget is removed possibly due to tearing and rubbing of the upper sheet. Figs. 8(a) and 8(c) show clearly the failure occurs very close to the outer circumference of the shoulder indentation.

Fig. 9 shows a cross sectional view and close-up views of a friction stir spot weld in a partially failed lap-shear specimen. The arrows in Fig. 9(a) schematically show the loading direction. The HAZ, the TMAZ, and the SZ are also indicated in Fig. 9(a). As shown in Fig. 9(a), near the upper right portion of the friction stir spot weld, marked as Leg 2, a crack (marked as point A) appears to emanate from the tip of a curved notch that terminates near the boundary of the SZ. However, no failure or damage can be seen in the lower left leg, marked as Leg 1, due to the different geometries of the nugget in the upper and the lower sheets, in contrast to the failure process of the resistance spot weld as shown in Lin et al. [14]. The failure of the friction stir spot weld in the lap-shear specimen may be initiated in the upper sheet near the middle part of the nugget, marked as point A and then propagates along the nugget circumference, marked as point B. Finally, the upper sheet is torn off with some part of the nugget, marked as point C. A similar failure mechanism was also observed in HSLA steel lap-shear specimens [15] and in mild steel square-cup specimens under combined opening and shear loading conditions [16].

Fig. 9(b) is a close-up view of region II shown in Fig. 9(a). In Fig. 9(c), a curved notch is shown near the right hand side of the weld nugget. The zigzag curved interface between the upper and lower sheet is shown in the square marked D. As shown in Fig. 9(c), the growth of the curved crack does not follow the zigzag curved interface. Fig. 9(d) is a close-up view of the zigzag curved interface in the square marked D in Fig. 9(c). Fig. 9(d) clearly shows that the location of the curved crack is not along the zigzag curved interface. It is possible that the curved crack growth occurring in the TMAZ near point A in Fig. 9(a)

is due to asymmetrical weld nugget geometry and inhomogeneous material properties in the TMAZ.

Five specimens are spot-friction-welded with the same processing parameters to assess the repeatability of the failure load and failure mechanism under the quasi-static tensile tests. The average of the failure loads of these five specimens under the loading is 4457 N. The maximum and minimum of these five failure loads are 4709 N and 4155 N, respectively. Observations of the micrographs of the cross sections of the five failed friction stir spot welds revealed that they have the same failure mechanisms under the loading conditions.

Based on a recent study of Lin et al. [14], the necking/shear failure mechanism is the principal failure initiation mechanism of the nugget pullout failure mode in lap-shear specimens from the mechanics viewpoint. Note that due to the limited ductility, a combined mode of necking and shear localization is the principal failure mechanism of aluminum 6111 sheets under biaxial stretching conditions as indicated in Chien et al. [17].

In order to understand the relationship between failure locations and microindentation hardness variations of the friction stir spot welds, microindentation hardness data across the BM, HAZ, TMAZ and SZ were obtained. Indentations were made with a spacing of 0.5 mm along each of the four parallel lines shown in Fig. 10(a). The four lines are parallel to the loading direction of the specimen shown in Fig. 2 and on the cross-section cut through the center of the weld. Fig. 10(b) shows the hardness variation traversing from the BM, across the HAZ and the TMAZ, and through the SZ. The hardness initially decreases upon approaching the boundary between the BM and the HAZ, then drops sharply to a minimum in the TMAZ. After passing the TMAZ, the hardness gradually increases up to the SZ hardness of about 90 Hv. The interface between the HAZ and TMAZ is the softest region according to Fig 10, where the cracks of friction stir spot

welds in the lap-shear specimens under the loadings initiate and lead to fracture of the specimens. Note that Liu et al. [13] reported that some of their friction-stir-welded joints of 2017-T351 aluminum alloy fractured in the softened regions near the interface between weld nuggets and TMAZs.

As also shown in Fig. 10(b), the BM is the hardest regions (approximately 120 Hv) of the specimen. This is contrary to predictions based on grain size arguments alone, which suggest the hardness maximum may occur in the SZ. The considerable softening of the material in the SZ in contrast to that in the BM can be explained by a significant reduction of dislocation density and precipitate distributions [18-21].

4. Conclusions

Microstructures and failure mechanisms of friction stir spot welds in aluminum 6061-T6 lap-shear specimens were investigated based on experimental observations. For friction stir spot welds made in this investigation, the circumferential failure mode or the nugget pullout failure mode was observed. The experimental results suggest that under lap-shear loading conditions, the failure is initiated near the SZ in the middle part of the nugget and the failure propagates along the circumference of the nugget to final fracture. The location of the initial necking/shear failure is near the possible original notch tip and the failures of the friction stir spot welds were fractured through the TMAZ near the weld nuggets. Based on the microindentation hardness measurements, the hardness initially decreases upon approaching the boundary between the base metal and the HAZ, then drops sharply to a minimum in the TMAZ. After passing the TMAZ, the hardness gradually increases up to the SZ hardness. The interface between the HAZ and the TMAZ is the softest region, where the cracks of friction stir spot welds in the lap-shear specimens under

the loadings initiate and lead to fracture of the specimens.

Acknowledgement

This project was supported by the National Science Council of the Republic of China under grant number NSC 94-2212-E-005-019. The authors would also like to express their appreciation to the staff of the metallurgy laboratory and the machining centers at National Chung Hsing University and Da Yeh University for their assistance.

References

[1] P.-C. Lin, S.-H. Lin, J. Pan, T. Pan, J.M. Nicholson, M.A. Garman, Microstructures and failure mechanisms of spot friction welds in lap-shear specimens of aluminum 6111-T4 sheets, SAE Technical Paper no. 2004-01-1330, Society of Automotive Engineering, Warrendale, PA., 2004.

[2] P. Thornton, A. Krause, R. Davies, Aluminum spot weld, Welding Journal 75 (1996) 101s-108s.

[3] A. Gean, S.A. Westgate, J.C. Kucza, J.C. Ehrstorm, Static and fatigue behavior of spot-welded 5182-0 aluminum alloy sheet, Welding Journal 78 (1999) 80s-86s.

[4] R. Sakano, K. Murakami, K. Yamashita, T. Hyoe, M. Fujimoto, M. Inuzuka, U. Nagao, H. Kashiki, Development of spot FSW robot system for automobile body members, in: Proceedings of the 3rd International Symposium of Friction Stir Welding, Kobe, Japan, 2001.

[5] T. Iwashita, Method and apparatus for joining, US Patent 6601751 B2, August, 5, 2003.

[6] C.J. Dawes, W.M. Thomas, Friction stir process welds aluminum alloys, Welding Journal 75 (1996) 41-45.

[7] D. Wang, S. Liu, Z. Cao, Study of friction stir welding of aluminum, Journal of Materials Science 39 (2004) 1689-1693.

[8] D.J. Waldron, R.G. Pettit, US Patent 6168067 (2001).

[9] W.M. Thomas, E.D. Nicholas, J.C. Needham, M.G. Murch, P. Temple-smith, C.J. Dawes, US Patent 5460317 (1995).

[10] D.-A. Wang, S.-C. Lee, Effect of welding force on failure loads of friction stir spot welds in aluminum 6061-T6 lap-shear specimens, to be submitted for publication, 2006.

[11] J.M. Sawhill, S.T. Furr, Spot weldibility tests for high-strength steels, SAE Technical Paper no. 810352, Society of Automotive Engineering, Warrendale, PA., 1981.

[12] Z. Lin, Y. Zhang, G. Chen, Y. Li, Study on real-time measurement of nugget diameter for resistance spot welding using a neuro-fuzzy algorithm, in Instrumentation and Measurement Technology Conference, Como, Italy, 18-20 May 2004, 2230-2233.

[13] H.J. Liu, H. Fujii, M. Maeda, K. Nogi, Tensile properties and fracture locations of friction-stir-welded joints of 2017-T351 aluminum alloy, Journal of Materials Processing Technology 142 (2003) 692-696.

[14] P.-C. Lin, S.-H. Lin, J. Pan, Modeling of plastic deformation and failure near spot welds in lap-shear specimens, SAE Technical Paper no. 2004-01-0817, Society of Automotive Engineering, Warrendale, PA., 2004.

[15] S. Zuniga, S.D. Sheppard, Resistance spot weld failure loads and modes in overload conditions, Fatigue and Fracture Mechanics: 27th Volume, ASTM STP 1296, Piascik, R. S., Newman, J. C., and Dowling, N. E., Eds., American Society for Testing and Materials, (1997) 469-489.

[16] S.-H. Lin, J. Pan, T. Tyan, P. Prasad, A general failure criterion for spot welds under combined loading conditions, International Journal of Solids and Structures 40 (2003) 5539-5564.

[17] W.Y. Chien, J. Pan, S.C. Tang, A combined necking and shear localization analysis for aluminum sheets under biaxial stretching conditions, International Journal of Plasticity 20 (2004) 1953-1981.

[18] G. Liu, L.E. Murr, C.-S. Niou, J.C. McClure, F.R. Vega, Microstructural aspects of the friction-stir welding of 6061-T6 aluminum, Scripta Materialia 37 (1997) 355-361.

[19] L.E. Murr, G. Liu, J.C. McClure, A TEM study of precipitation and related microstructures in friction-stir-welded 6061 aluminum, Journal of Materials Science 33 (1998) 1243-1251.

[20] M. Boz, A. Kurt, The influence of stirrer geometry on bonding and mechanical properties in friction stir welding process, Materials and Design 25 (2004) 343-347.

[21] C. Genevois, A. Deschamps, A. Denquin, B. Doisneau-cottignies, Quantitative investigation of precipitation and mechanical behaviour for AA2024 friction stir weld, Acta Materialia 53 (2005) 2447-2458.

Table 1
Chemical compositions (wt.%) of 6061-T6 aluminum sheets

Mg	1.00
Si	0.59
Fe	0.51
Cu	0.30
Cr	0.22
Mn	0.05
Ti	0.02
Zn	<0.01
Al	Rem.

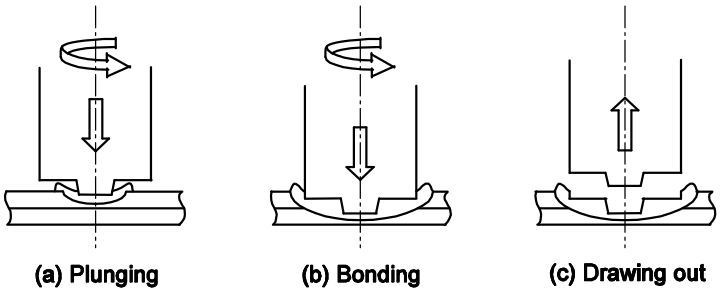

Fig. 1. A schematic illustration of friction stir spot welding process.

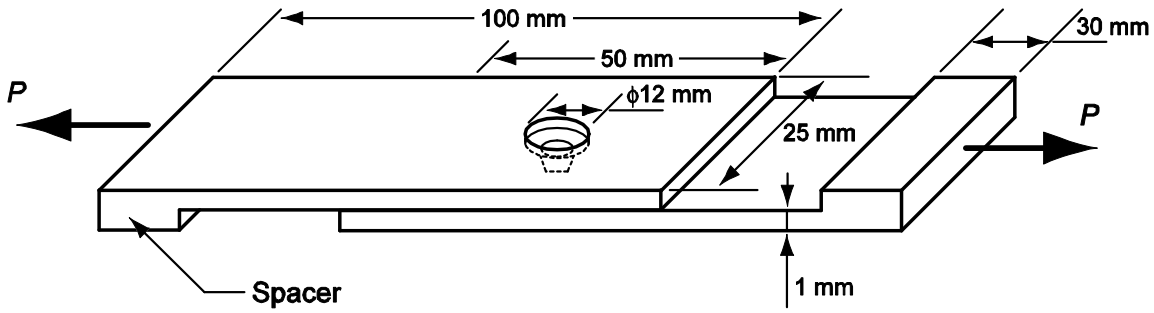

Fig. 2. A schematic plot of a lap-shear specimen and the applied force *P* shown as the bold arrows.

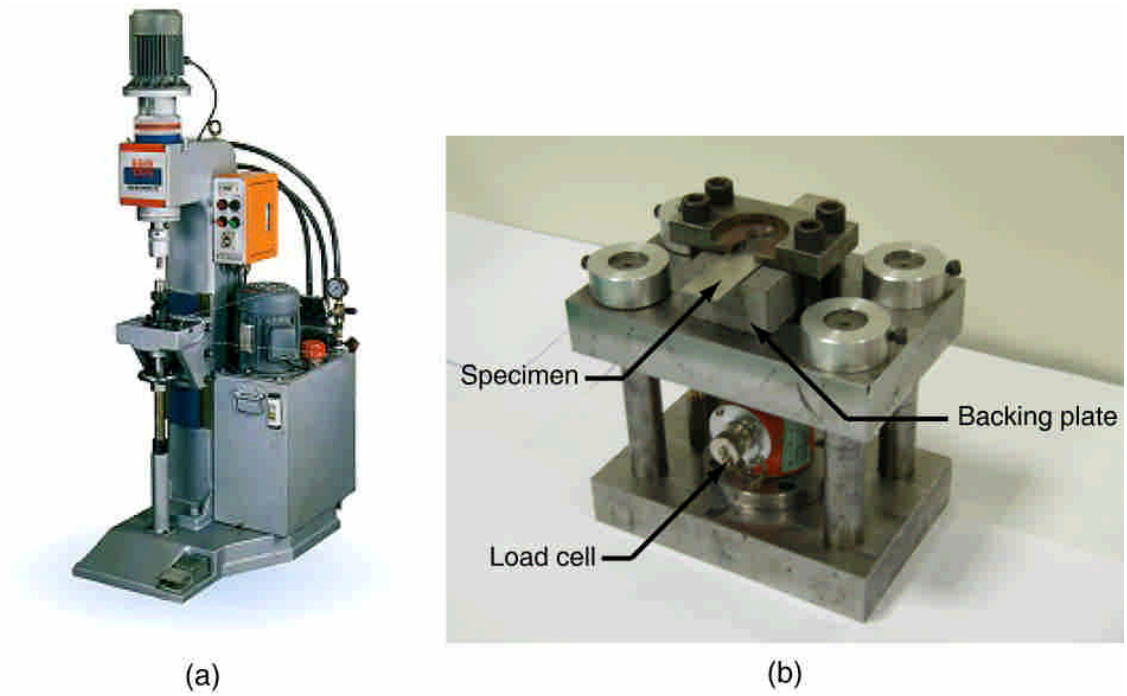

Fig. 3. (a) A hydraulic riveting machine for friction stir spot welding. (b) A close-up view of the tool and the specimen fixture.

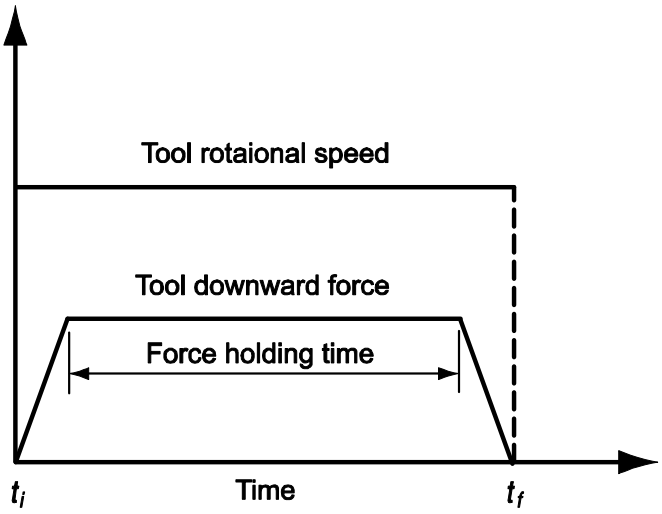

Fig. 4. A schematic plot of the processing parameters as a function of time.

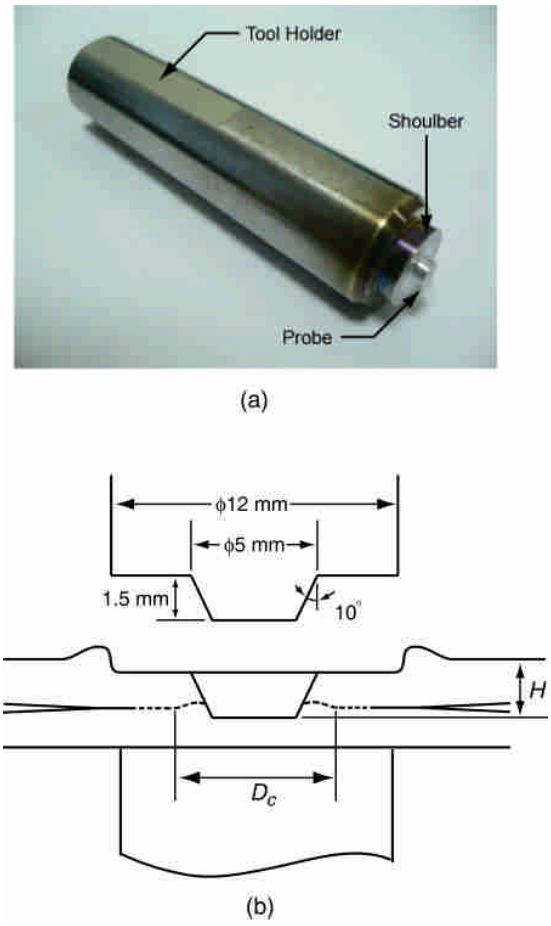

Fig. 5. (a) A photo of a tool. (b) A schematic plot of an extracted tool and two welded sheets after welding.

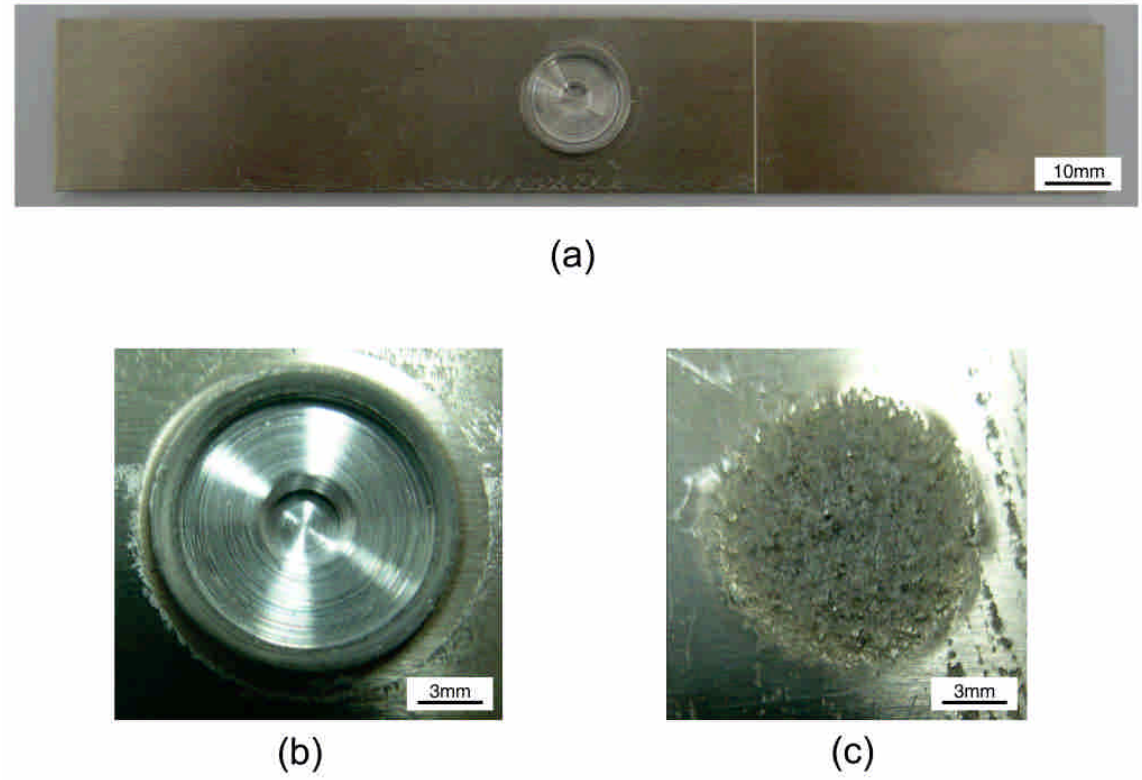

Fig. 6. (a) A lap-shear friction stir spot weld specimen of aluminum 6061-T6, (b) a close-up view of the friction stir spot weld on the upper sheet, (c) a close-up view of the friction stir spot weld on the lower sheet.

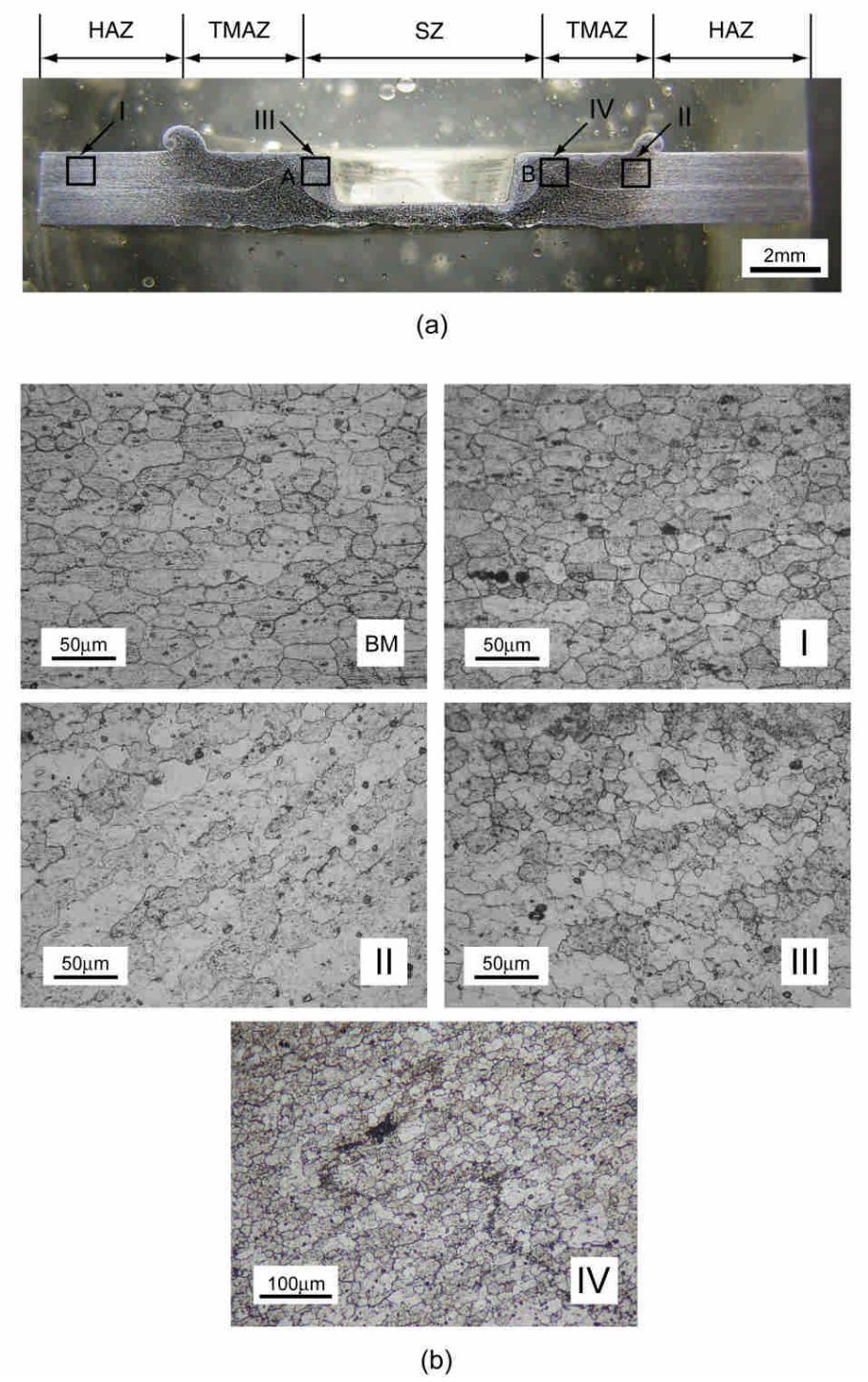

Fig. 7. (a) A micrograph of the cross section of a friction stir spot weld made by the tool, (b) close-up views of regions I, II, III and IV.

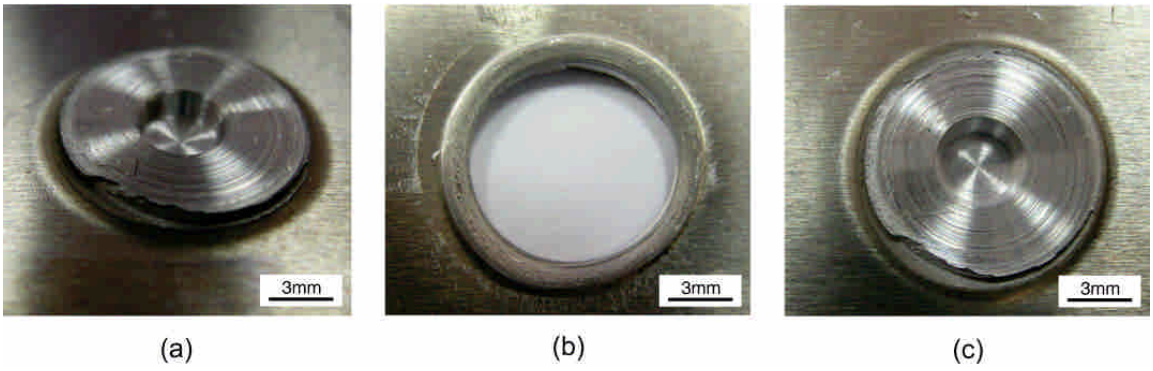

Fig. 8. (a) A failed friction stir spot weld lap-shear specimen, (b) a top view of a friction stir spot weld on the upper sheet of the failed specimen, (c) a top view of a friction stir spot weld on the lower sheet of the failed specimen.

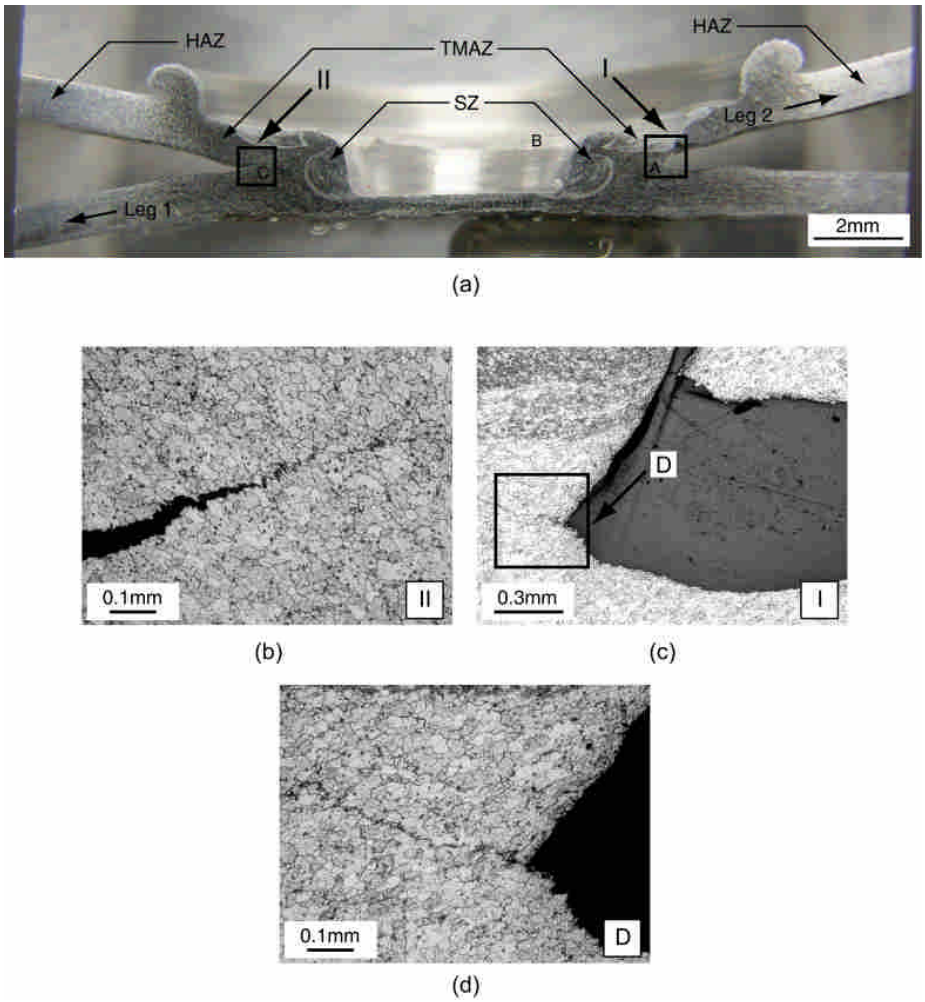

Fig. 9. (a) A micrograph of the cross section of a friction stir spot weld in a partially failed lap-shear specimen, (b) a close-up view of region II, (c) a close-up view of region I, (d) a close-up view of the region marked in the square D.

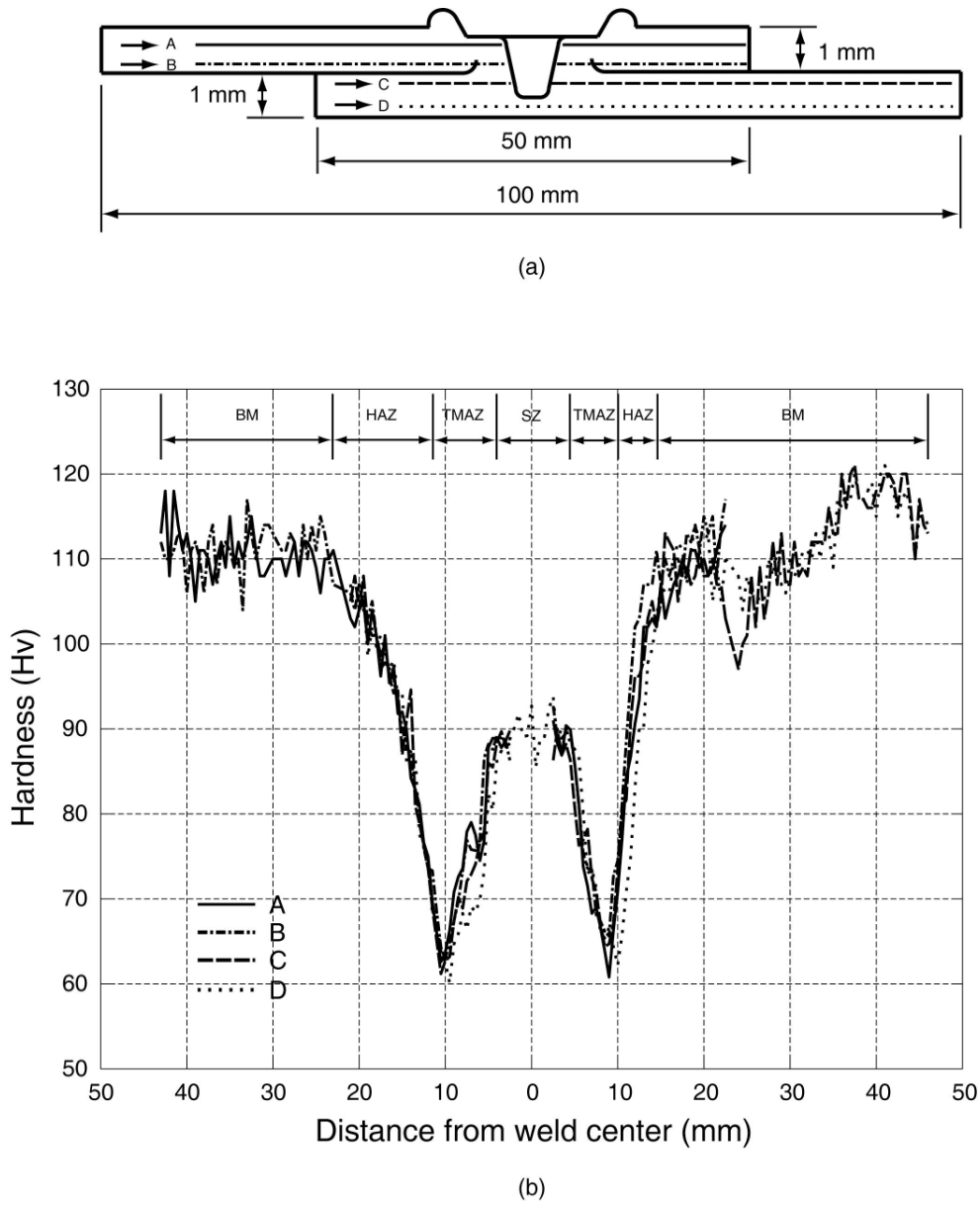

Fig. 10. (a) Locations of four horizontal hardness traverses. (b) Hardness profiles.